(U) Stand-off 3D Face Imaging and Vibrometry for Biometric Identification using Digital Holography

September 2009

Brian Redman, Joseph Marron, Nathan Seldomridge, Taylor Grow, Thomas Höft, John Novotny, Samuel T. Thurman, Carl Embry, and Andrew Bratcher

Lockheed Martin Coherent Technologies
135 S. Taylor Ave., Louisville, CO 80027

Richard Kendrick

Lockheed Martin Space Systems Company
AFAS
3251 Hanover Street
Palo Alto, CA 94304

ABSTRACT

Lockheed Martin Coherent Technologies (LMCT) has demonstrated 3D face imaging at ~ 1-2 mm lateral resolution and range precision at stand-off distances up to 100 m using digital holography. LMCT has also demonstrated the digital holography technique in a multi-pixel vibrometry mode in the laboratory. In this paper, we report on 3D face imaging using multiple-source (MS) and multiple-wavelength (MW) digital holography breadboards. We will briefly discuss the theory of 3D imaging using MS and MW digital holography with references to the literature. We will also briefly discuss the theory of vibrometry using a digital holographic setup. We then describe our implementation of these techniques in breadboard setups operating at 1550 nm wavelength (for MS digital holography) and at wavelengths near 1617 nm (for MW digital holography). We also present experimental results for 3D imaging and for vibrometry with these digital holographic setups.

1.0 Introduction

Lockheed Martin Coherent Technologies (LMCT) has demonstrated 3D face imaging at ~ 1-2 mm lateral resolution and range precision at stand-off distances up to 100 m using digital holography. LMCT has also demonstrated the digital holography technique in a multi-pixel vibrometry mode in the laboratory. In this paper, we report on 3D face imaging using multiple-source (MS) and multiple-wavelength (MW) digital holography breadboards. We will briefly discuss the theory of 3D imaging using MS and MW digital holography with references to the literature. We will also briefly discuss the theory of vibrometry using a digital holographic setup. We then describe our implementation of these techniques in breadboard setups operating at 1550 nm wavelength (for MS digital holography) and at wavelengths near 1617 nm (for MW digital holography). We also present experimental results for 3D imaging and for vibrometry with these digital holographic setups.

2.0 Multiple-Source (MS) and Multiple-Wavelength (MW) Digital Holography

The method of 3D shape measurement by multiple-source (MS) and by multiple-wavelength (MW) holography was invented by Haines and Hildebrand in 1965-1966.[1,2] The MS holographic technique is also known as the multiple-illumination-angle or multiple-illumination-point holographic method in the literature. The extension of multiple-wavelength holographic contouring to many-wavelength or broadband digital holographic laser radar (HLR) for fine-resolution 3D imaging in the optical regime was first discussed by Farhat in 1980[3], and experimentally demonstrated extensively by Marron and Schroeder in 1992-1993[4,5,6]. The textbooks by Schnars and Jueptner[7], and by Hariharan[8] describe both MS and MW holography in the cases of two sources and two wavelengths, respectively.

In addition to categorizing the holographic method as MS or MW, there are two holographic configurations that we have been investigating called pupil plane (PP) and image plane (IP) holography. Therefore, the configurations we are investigating are MS-PP, MS-IP, MW-PP, and MW-IP. MS digital holographic configurations have range resolutions that degrade with range for fixed offset distance between the two illumination sources, and between the sources and the receiver aperture. MW digital holographic configurations, on the other hand, have range resolutions that are constant with range, and set by the separation between the wavelengths used. In this paper, we will discuss only the MS-PP and MW-IP configurations, and the experimental results for the breadboards built in these configurations.

The conceptual diagrams for the MS-PP (with two sources) and the MW-IP (with two wavelengths) digital holographic configurations are shown in figures 1 (a) and 1 (b), respectively.

In the MS-PP configuration with two sources as shown in figure 1 (a.), a 1x2 splitter splits off part of the laser output to a local oscillator (LO) fiber, and the other part of the laser output is switched between two fibers, the output ends of which are at two different locations at the focus of the transmitter's objective lens. The output of the LO fiber propagates with the received laser light from the image of the object (i.e., with the object beam) and interferes with this object beam to form a hologram at the focal plane array (FPA) of the camera. A hologram is formed for each source position by switching between the two source fibers, whose outputs are at the focus of the transmitter lens, for two sequential frames.

The effective focal length of the receiver optics and the placement of the camera's FPA are arranged so that the FPA would be imaged onto the entrance pupil plane of the receiver optics in back-propagating from the FPA, hence the designation Pupil Plane holography. In this configuration, in the absence of aberrations and for a sufficiently large physical clear aperture, the system performs as if there were a large FPA (the same size as the physical FPA magnified by the receiver optics) at the pupil plane with no receiver optics, and as if the point source LO/reference beam originated at the object. Thus, this configuration is equivalent to a lensless Fourier transform holography setup.[9]

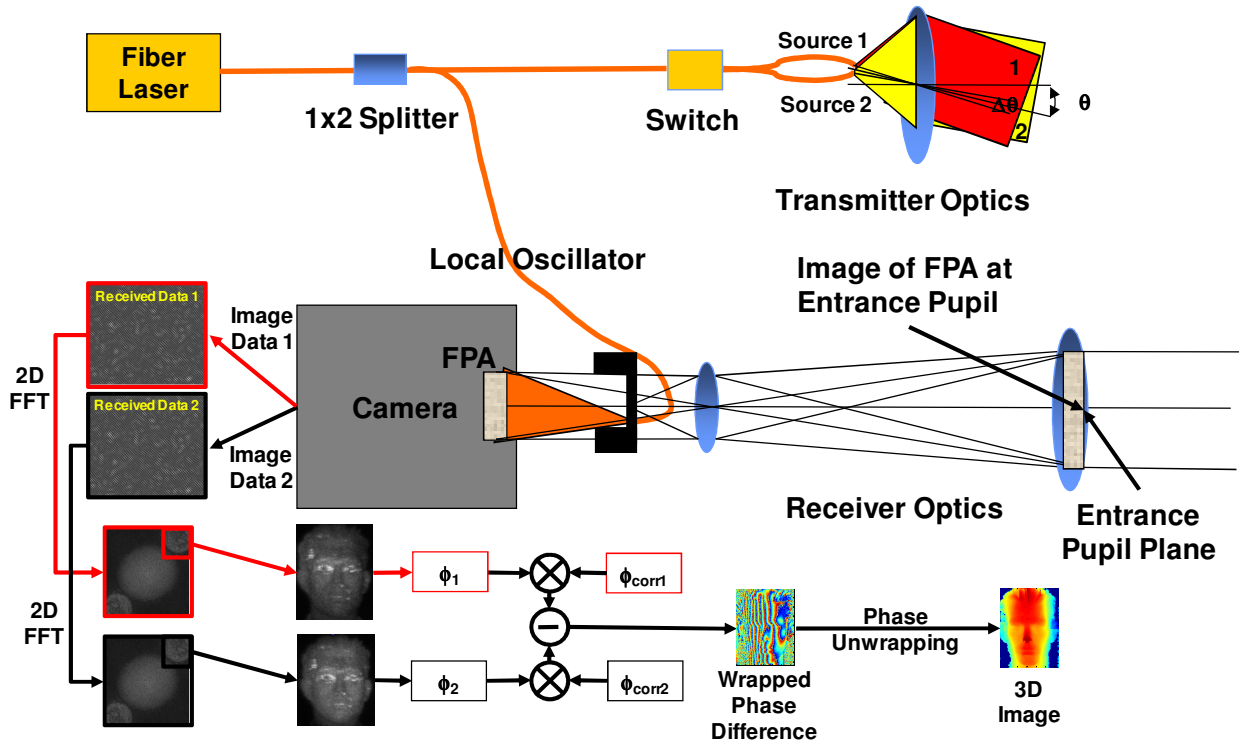

(a.)

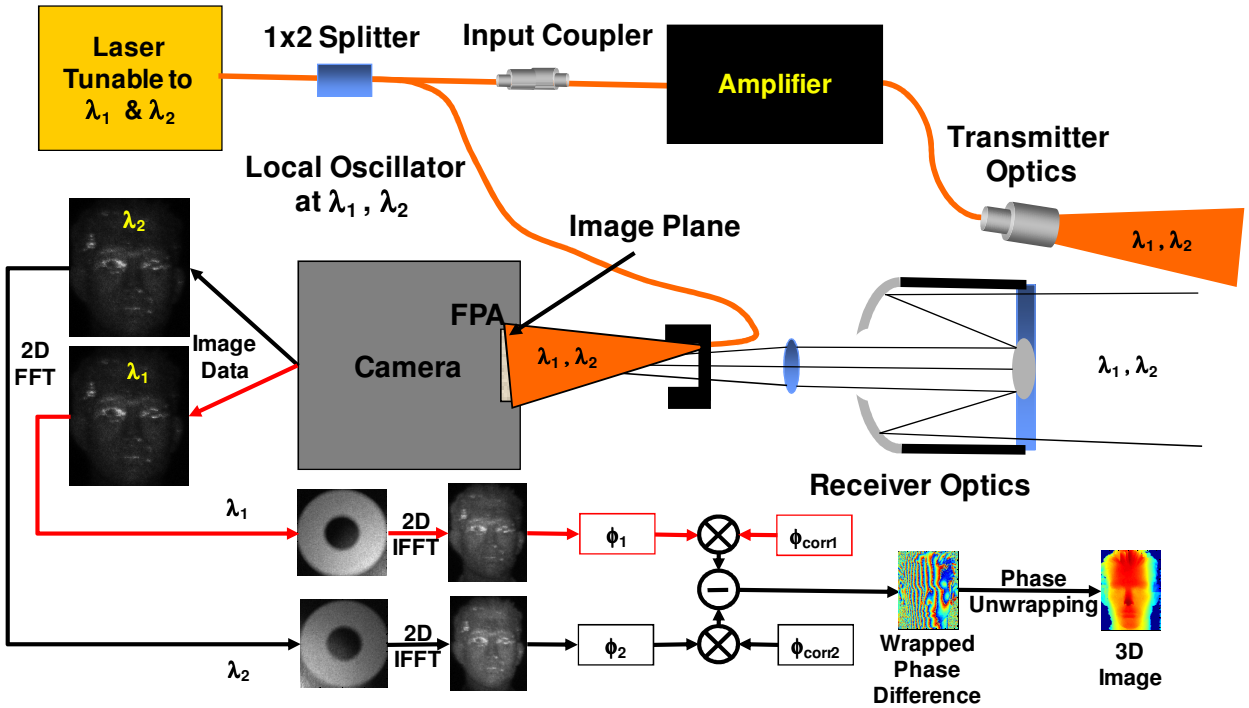

(b.)

Figure 1. (a.) Multiple-Source-Pupil Plane (MS-PP) digital holography configuration for two sources, and (b.) Multiple-Wavelength-Image Plane (MW-IP) digital holography configuration for two wavelengths.

Each MS-PP digital hologram consists of a speckle pattern, and within each speckle correlation cell is a fringe pattern due to the interference of the LO with the object beam. For each MS-PP digital hologram, the fringe period (and equivalently, the fringe spatial frequency) and fringe orientation are determined by the angle between the LO and the object beam. By taking the 2D Fast Fourier Transform (FFT) of each of the MS-PP digital holograms recorded from the two different sources, a complex image of the object and its complex conjugate image are formed for each MS-PP digital hologram. One of the complex images for each source is extracted (i.e., the complex conjugate image is not used). Each complex image can be represented by a magnitude and phase for each pixel in the image data array. The phases for each pixel in the complex image for each source are extracted, and the phase differences for corresponding pixels between the two complex images from the two sources are computed. The phase difference for each pixel is proportional to the range for that pixel to within a phase/range ambiguity interval (see below for the description of the phase/range ambiguity interval). Conversion of this phase difference image to a range image provides the desired 3D image of the object. Note that prior to taking the phase difference, a phase image designed to correct for system and atmospheric aberrations can be multiplied by the phase image for each source location.[10,11]

In the MW-IP configuration shown in figure 1 (b.) with two wavelengths, the laser tunes between two wavelengths which are set so that their frequency difference provides a user-selected unambiguous range (see below for more on setting the desired unambiguous range). A 1x2 splitter splits the laser output into an LO/reference beam and a transmitted beam that illuminates the object. Note that transmitted beam may be amplified as shown in figure 1 (b.) to provide enough power for a given operational range.

In the MW-IP configuration, the receiver optics image the received laser light scattered by the object onto the camera FPA located at the image plane of the receiver optical system to form the object beam. The interference of the LO/reference beam at each wavelength with the corresponding object beam at the same wavelength is recorded as an image plane digital hologram for that wavelength. A 2D FFT is performed on the digitally recorded image plane hologram for each wavelength. This produces a complex image and its complex conjugate image of the pupil plane for each wavelength. For each wavelength, only one complex image of the pupil plane is extracted, and the 2D inverse FFT (IFFT) is performed on this extracted complex image to form a complex image of the target for each wavelength. The processing of the complex target images at the two wavelengths proceeds as described above for the complex target images for the two source locations in the MS-PP method to produce a 3D image of the target.

As mentioned above, there are range ambiguities in the range measurement due to the 2π-radian periodicity of the phase difference. The unambiguous range, ΔR, is determined by the change in range between adjacent fringes in the hologram, which corresponds to a 2π-radian phase change, and for the two-wavelength digital holography case is given by[12]

$$\Delta R = \frac{\lambda_1 \cdot \lambda_2}{2 \cdot |\lambda_1 - \lambda_2|} = \frac{\Lambda}{2} \qquad (1)$$

where $\lambda_{1(2)}$ = wavelength 1 (2),
Λ = synthetic or equivalent wavelength

For the case of two-source digital holography, the unambiguous range is given by[13],

$$\Delta R = \frac{\lambda}{\sin(\theta) \cdot \sin(\Delta\theta)} = \frac{\Lambda}{2} \qquad (2)$$

where λ = wavelength
$\Delta\theta$ = angle between the two illumination source directions
θ = angle between the bisector of $\Delta\theta$ and the optical axis of the receiver (it is assumed that $\Delta\theta$ is much smaller than θ).

As is the case for single tone amplitude modulation and for two-frequency continuous wave radar ranging, the unambiguous range and the range resolution for MW and MS holography with two wavelengths and two sources, respectively, are equal to half the modulation wavelength, which in these cases are the synthetic or equivalent wavelengths shown in equations (1) and (2), respectively.[14]

The range measurement precision (i.e., the range measurement standard deviation) is given by[15]

$$\sigma_{Range} = \frac{c}{4 \cdot \pi \cdot \Delta F \cdot \sqrt{SNR}} = \frac{\Lambda}{4 \cdot \pi \cdot \sqrt{SNR}} = \frac{\Delta R}{2 \cdot \pi \cdot \sqrt{SNR}} \quad (3)$$

where c = speed of light
ΔF = frequency difference between the two wavelengths for 2-λ digital holography
Λ = synthetic or equivalent wavelength (see equations (1) and (2)) = $c/\Delta F$
SNR = electrical power signal-to-noise ratio = peak current or voltage squared divided by the variance of the current or voltage noise.
ΔR is given by equation (1) or (2) for two-wavelengths or two-sources, respectively.

Thus, the range measurement precision can be improved (made smaller) by decreasing ΔR (by increasing $\Delta\lambda = |\lambda_1 - \lambda_2|$ for 2-λ digital holography, or by increasing θ and/or $\Delta\theta$ for 2-source digital holography), and/or by increasing the SNR. Making ΔR too small, however, introduces problems with correctly unwrapping the phase in high slope areas of the object, e.g., the edges of the nose on a face.

The noise contributions to the SNR are mainly due to signal shot noise and speckle noise. In the absence of speckle, the SNR is equal to the carrier-to-noise ratio (CNR) which is improved by setting the LO high enough to overcome receiver and background light noise so that the receiver becomes signal shot noise limited. The CNR can also be improved by increasing the backscattered laser power received from the target. The CNR for our configuration with the LO set to dominate all other noise sources is given by

$$\mathrm{CNR} = \frac{\eta \cdot T_{opt} \cdot E_p \cdot \lambda^3 \cdot \rho}{4 \cdot h \cdot c \cdot \pi \cdot D_{tgt}^2} \cdot e^{-2 \cdot \alpha_{atm} \cdot R} \quad (4)$$

where η = detector quantum efficiency,
T_{opt} = the round-trip transmission of the transceiver optics,
E_p = the output laser pulse energy,
λ = laser wavelength,
ρ = target reflectance at the laser wavelength,
h = Planck's constant,
c = the speed of light,
D_{tgt} = the target diameter,
α_{atm} = atmospheric extinction coefficient,
R = Range.

Note that the only dependence of CNR on range is through the atmospheric transmission losses since we insure in our setups that the receiver's physical clear aperture diameter is greater than or equal to the diffraction-limited coherent aperture diameter for the target diameter and longest operating range for which the system is designed.

The single frame SNR degradation due to speckle noise cannot be improved by increased received laser power since for large CNR the single frame SNR saturates to 1 (see equation (5) below). Speckle noise limited SNR can be improved by spatial, temporal, spectral, and/or polarization averaging. For coherent detection, however, the mixing efficiency for each detector is optimized for reception in a single spatial, spectral, and polarization mode, so that when using a single imaging receiver, temporal averaging is the

simplest approach for speckle noise reduction. As the target moves, the speckle pattern at the FPA moves so that different frames will capture different speckle patterns in the holograms, and the complex images formed from these different frames can be averaged together to reduce speckle noise.

In practice, we have found that averaging 16-32 frames of different speckle realizations produces acceptable 3D imagery. With frame averaging, the image or irradiance SNR is given by

$$\mathrm{SNR} = \frac{\mathrm{CNR}^2}{1 + 2\cdot\mathrm{CNR} + \dfrac{\mathrm{CNR}^2}{\mathrm{N_{frames}}}} \qquad (5)$$

where $\mathrm{N_{frames}}$ = the number of image frames averaged.

As mentioned above, the phase image ambiguity of $2\cdot\pi$ must be unwrapped to a continuous phase image in reconstructing the 3D image. After applying an unwrapping algorithm to produce a continuous phase image, $\Delta\phi(x,y)$, this phase image is scaled to a distance image, where the distance with pixel position, z(x,y), is given by

$$z(x,y) = \frac{\Delta\phi(x,y)}{2\cdot\pi}\cdot\frac{\lambda}{\sin(\theta)\cdot\sin(\Delta\theta)}, \text{ for 2-source digital holography,} \quad (6)$$

or

$$z(x,y) = \frac{\Delta\phi(x,y)}{2\cdot\pi}\cdot\frac{\lambda_1\cdot\lambda_2}{2\cdot\left|\lambda_1-\lambda_2\right|}, \text{ for 2-}\lambda\text{ digital holography.} \quad (7)$$

Aberrations due to the system optics and the atmosphere can be corrected digitally by applying phase corrections to the phase image.[16,17]

3.0 Vibrometry with MS-PP Digital Holography

Commercial-off-the-shelf (COTS) single detector coherent laser vibrometers have previously been used for voice and heartbeat capture from human subjects, but the subjects were required to be cooperative and stationary, and the capture was done at relatively short ranges.[18,19] LMCT has previously captured intelligible voice data from a human subject at short range with a single detector coherent ladar vibrometer. We have also recently captured single tone data from a speaker using the PP digital holography configuration operating at 1550 nm wavelength with a high frame rate, short wavelength infrared (SWIR) camera. We show this data below after describing the technical principles involved.

The basic principle underlying coherent laser vibrometry is that the velocity of a vibrating surface Doppler shifts the frequency of the backscattered laser light. A portion of this backscattered light is optically mixed with fixed frequency laser light (the LO) that is phase coherent with the laser light illuminating the target. The difference frequency (beat frequency) between the LO and the Doppler shifted backscattered laser light is detected using a photodetector. This signal can be processed to extract surface vibration frequency and amplitude data. For vibrometry, only one laser wavelength is needed.

One can consider the coherent ladar vibrometer to be an interferometer with a single pixel receiver. As the intensity fringe pattern formed by the interference between the LO beam and the signal beam moves across the detector due to target motion, the detector's output current is modulated. Note that for most single pixel laser vibrometers, the LO beam and received beam are aligned to be coaxial and incident normal to the detector surface to maximize mixing efficiency, and in this configuration, the fringes move over the detector longitudinally, i.e., perpendicular to the detector surface. For our PP digital holography setup the LO beam is incident on the FPA at a small angle to the object beam (i.e., the received signal

beam) so that the fringes move laterally across the FPA. If the fringe pattern is oscillating back and forth due to target vibration, then a given detector's output current is also temporally modulated at the vibration frequency. If the single detector is replaced with an array of detectors, the interference fringes can be imaged by the array. This is what the staring array receiver does in the PP digital holography setup. At low enough vibration frequencies (under ~ 15 Hz) one can see the oscillation of the fringe pattern across the receivers FPA on a display. In this configuration, each detector sees a temporally oscillating intensity modulation at the vibration frequency, so the sensor acts as an array of coherent ladar vibrometers.

In human subjects, the voice and the heartbeat induce vibrations of the skin can be measured with a laser vibrometer. Voice and heartbeat signals have been shown to have characteristics that can separately identify individuals with moderately low error rates, even with fairly short data segments (~5-6 seconds for heartbeat and ~ 0.25 seconds to 5 seconds for voice).[20,21] Unlike acoustic and radar vibration sensors, the small beamwidth of the laser ensures that the vibration signals come only from the subject and not from others nearby so that voice and heartbeat signatures from a single individual can be spatially isolated from the signatures other individuals in a crowd.

The same general equations for the CNR and SNR presented in section 2.0 for 3D imaging apply to the vibrometry case, but the number of illuminated pixels from which data is collected is smaller for vibrometry mode. Preliminary modeling indicates the long range breadboard will be capable of operating in vibrometry mode out to at least 1 km in clear air.

4.0 Experimental Results

We initially built a cw laser MS-PP digital holography breadboard system operating at 1550 nm wavelength with two source positions as shown in figure 1 (a.). With this breadboard we collected 3D imagery of a mannequin face at 4.6-m range in the lab. Using a 2-λ MW-IP digital holography setup, we collected 3D face images at 100 m range. Finally, using only one of the sources at a single wavelength in the cw MS-PP based breadboard, and replacing the relatively low frame rate original SWIR band camera with a high frame rate SWIR band camera, we collected vibrometry data from a speaker at short range in the laboratory as a proof-of-principle demonstration of the vibrometry capability of the PP digital holography configuration. The results of these three experiments are presented in the next three subsections.

4.1. Multiple Source Pupil Plane (MS-PP) 3D Imaging Results

We built a breadboard in the two-source MS-PP digital holography configuration shown in figure 1 (a.). The transmitted beam illuminated a mannequin face at 4.6-m range with a transmitter-to-receiver angle, θ, of 15°, and an angle between the sources optical axes, Δθ, of 86 μrad yielding an unambiguous range, ΔR, of 7 cm. Figure 2 shows three rotations of the 3D image of the mannequin face from a data set captured in this experiment. Sixteen frames of different speckle realizations were averaged together for this data set. A color digital image of the mannequin face captured at the same time is draped onto the reconstructed 3D surface. Note that various mm-scale bumps and scrapes were applied to the mannequin face to demonstrate the mm-scale precision of the 3D reconstruction.

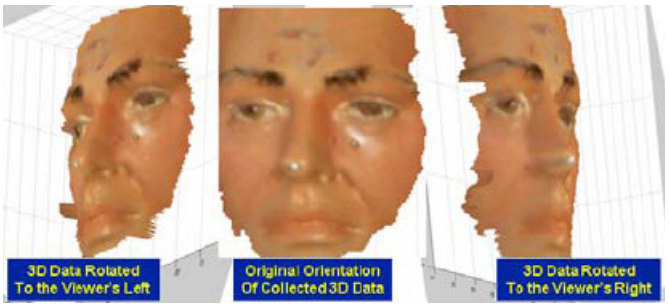

Figure 2. 3D mannequin face data collected with a 2-source pupil plane digital holographic sensor at 4.6-m range.

4.2. Multiple Wavelength Image Plane (MW-IP) 3D Imaging Results

The 2-λ MW-IP digital holography setup at LMCT's Table Mountain field test facility was used to capture 3D face images at 100 m range. The setup operated with two wavelengths near 1617 nm with an offset of ~0.065 nm between the two wavelengths, providing an unambiguous range of ~ 2 cm. Figure 3 (a.) shows the unwrapped phase image scaled to a pseudo-color range image with the color scale on the right in units of meters. Figure 3 (b.) shows the reconstructed 3D image with a color digital image of the mannequin face draped onto the 3D surface in the face-on view, and figure 3 (c.) shows this 3D image rotated to profile view.

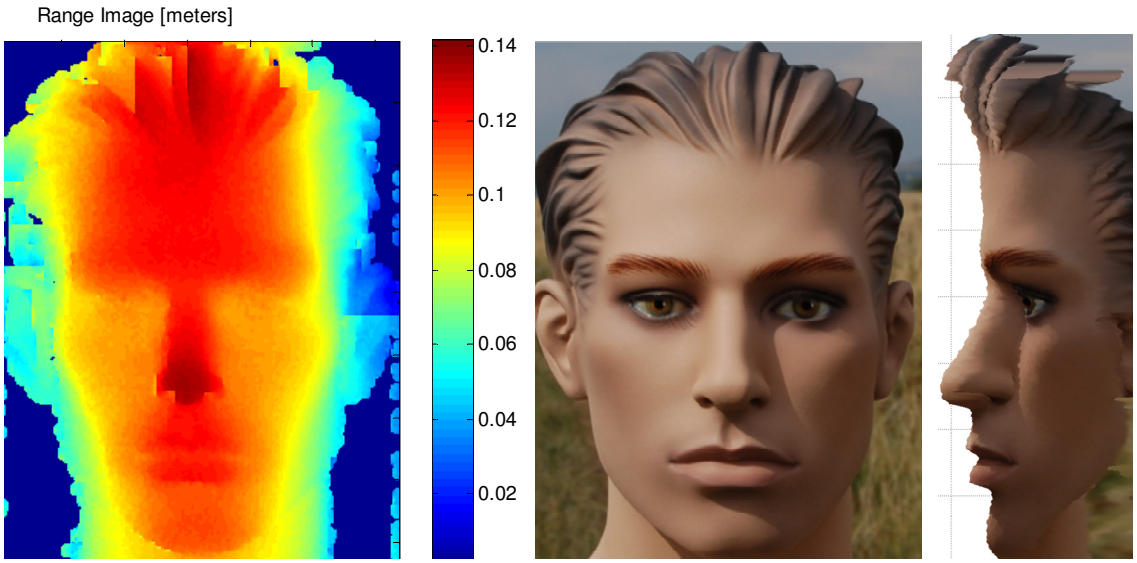

Figure 3. 2-λ image plane digital holography 3D face imaging results at 100 m range: (a.) the unwrapped phase image scaled to a pseudo-color range image with the color scale on the right in units of meters, and (b.) the reconstructed 3D image with a color digital image of the mannequin face draped onto the 3D surface in face-on view, and (c.) the 3D image in (b.) rotated to profile view.

4.3. Pupil Plane (PP) Vibrometry Results

Figure 4 shows data from the initial experiment with a laboratory setup of the vibrometry mode in the single-wavelength PP digital holography configuration. In this experiment, the target was a stationary speaker voice coil being driven with a 10 Hz sinusoidal tone. The breadboard was setup in the PP digital holography configuration. The target was 46 cm from the receiver aperture. We chose 10 Hz vibration frequency for this initial test so that we could visually verify the oscillatory motion of the fringes on the real-time computer display of the SWIR camera's output. The sinusoidal signal extracted from the captured digital holography data and the peak at 10 Hz in the magnitude spectrum (log scale) of this signal for this initial experiment are easily seen in the graphs shown in figure 4.

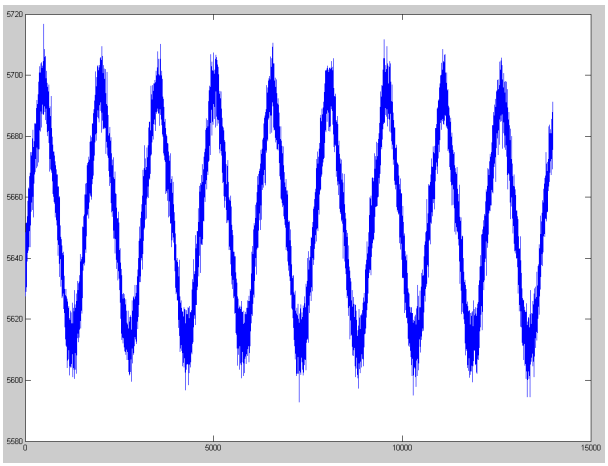

x-axis is in time samples of
65.78 µs per sample

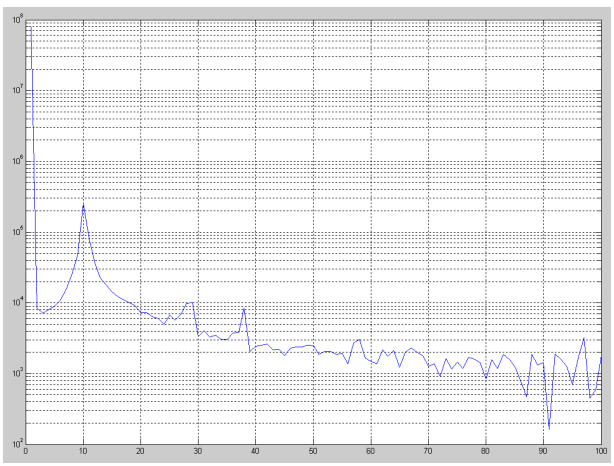

x-axis is in frequency samples
of 1.086 Hz per sample

Figure 4. First laboratory test data of the pupil plane digital holography setup operating in vibrometry mode. The 10 Hz sinusoidal tone signal applied to the speaker target is clearly visible with good SNR in this data.

5.0 Summary

Lockheed Martin Coherent Technologies (LMCT) has demonstrated 3D face imaging at ~ 1-2 mm lateral resolution and range precision at stand-off distances up to 100 m using digital holography. LMCT has also demonstrated the digital holography technique in a multi-pixel vibrometry mode in the laboratory. In this paper, after briefly discussing the theory of multiple source (MS) and multiple wavelength (MW) digital holography for 3D image capture and for single wavelength, multi-pixel vibrometry, in the pupil plane (PP) and image plane (IP) holographic configurations, we presented experimental results for 3D image capture at close range (4.6 m) in the two-source MS-PP digital holography configuration, for vibrometry at very close range (46 cm) in the single-wavelength PP digital holography configuration, and for 3D image capture at long range (100 m) in the two-wavelength MW-IP digital holography configuration. These experiments constitute initial proof-of-principle for the capability of a digital holography setup to capture both 3D imagery and vibrometry data as needed for a multi-modal 3D face + voice + heartbeat capture sensor for biometric identification and intent detection.

6.0 Acknowledgements

The work reported herein was supported by Lockheed Martin internal research and development (IR&D) funding.

7.0 References

[1] Haines, K.A., and B. P. Hildebrand, Phys. Letters **19, 10** (1965); **20, 422** (1966).

[2] Hildebrand, B.P., and Haines, "Multiple-Wavelength and Multiple-Source Holography Applied to Contour Generation, JOSA, Vol. 57, Number 2, February, 1967.

[3] Farhat, N.H., in Optics in Four Dimensions-1980, (M. A. Machado and L. M. Narducci, eds.), New York: American Institute of Physics, 1981, pp. 627-642.

[4] Marron, J.C. and K.S. Schroeder, Appl. Opt., 31, 255, 1992.

[5] Marron, J.C. and T.J. Schulz, Opt. Lett. 17, 285, 1992.

[6] Marron, Joseph C. and Kirk S. Schroeder, "Holographic laser radar," Opt. Lett., 18, 5, 1993.

[7] Schnars, Ulf and Werner Jueptner, Digital Holography – Digital Hologram Recording, Numerical Reconstruction, and Related Techniques, Springer-Verlag, 2005, pp. 31-35, 66-68, 86-92.

[8] Hariharan, P., Optical Holography, Principles, Techniques, and Applications, Cambridge University Press, 1996, pp. 285-289.

[9] Doval, Angel F. and Cristina Trillo, "Hybrid optonumerical quasi Fourier transform digital holographic camera," Speckle06: Speckles, From Grains to Flowers. Pierre Slangen and Christine Cerruti (eds.), Proc. SPIE Vol. 6341, 2006, pp. 63410Z-1 – 63410Z-6.

[10] Thurman, S.T., and J. R. Fienup, "Phase-error correction in digital holography," J. Opt. Soc. Am. A 25, 983-994 (2008).

[11] Marron, J.C., R.L. Kendrick, N. Seldomridge, T. Grow and T.A. Höft, "Atmospheric turbulence correction using digital holographic detection: experimental results," Optics Express, 17, 11638-11651 (2009) .

[12] Schnars and Jueptner, op. cit., pp. 32-33.

[13] Hariharan, op. cit., p. 288.

[14] Skolnik, Merrill I., Introduction to Radar Systems, New York: McGraw-Hill Book Company, Inc., 1962, p. 108.

[15] Skolnik, op. cit., p. 109.

[16] Thurman and Fienup, loc. cit.

[17] Marron, Kendrick, Seldomridge, Grow and Höft, loc. cit.

[18] Lai, Po-Hsiang, et. al., "A Robust Feature Selection Method for Noncontact Biometrics Based on Laser Doppler Vibrometry," IEEE Computer Society, Proc. of the 2008 Biometrics Symposium, September 2008, pp. 65-70.

[19] Zhu, Zhigang, Weihong Li and George Wolberg, "Integrating LDV Audio and IR Video for Remote Multimodal Surveillance," Proc. of the 2005 IEEE Computer Soc. Conf. on Computer Vision and Pattern Recognition, 2005.

[20] Kwon, Soonil and Shrikanth Narayanan, "Robust speaker identification based on selective use of feature vectors," Pattern Recognition Letters 28, 2007, pp. 85–89.

[21] Lai, et. al., op. cit., p. 70.